Human Brown Fat Radiodensity Indicates Underlying Tissue Composition and Systemic Metabolic Health

Mueez U Din,[1,2] Juho Raiko,[1,2] Teemu Saari,[1,2] Virva Saunavaara,[1] Nobu Kudomi,[3] Olof Solin,[4] Riitta Parkkola,[5] Pirjo Nuutila,[1,2] and Kirsi A. Virtanen[1,2]

[1]Turku PET Centre, Turku University Hospital, 20520 Turku, Finland; [2]Turku PET Centre, University of Turku, 20520 Turku, Finland; [3]Department of Medical Physics, Faculty of Medicine, Kagawa University, Kagawa 761-0793, Japan; [4]Turku PET Centre, Department of Chemistry, University of Turku and Accelerator Laboratory, Åbo Akademi University, 20520 Turku, Finland; and [5]Department of Radiology, Turku University Hospital and University of Turku, 20520 Turku, Finland

Context: Metabolic imaging studying brown adipose tissue (BAT) physiology has increased, in which computed tomography (CT) is commonly used as an anatomical reference for metabolic positron emission tomography (PET) imaging. However, the capacity of CT to provide metabolic information has been underexploited.

Objective: To evaluate whether CT radiodensity of BAT could noninvasively estimate underlying tissue morphology, regarding amount of stored triglycerides. Furthermore, could the alteration in tissue characteristics due to cold stimulus, as a marker for active BAT, be detected with radiodensity? Can BAT be differentiated from white adipose tissue (WAT) solely using CT-based measurements?

Design, Setting, and Participants: A cross-sectional study evaluating 66 healthy human subjects with CT, PET, and [1]H-magnetic resonance spectroscopy (^{1}H-MRS).

Main Outcome Measures: BAT radiodensity was measured with CT. BAT-stored triglyceride content was measured with ^{1}H-MRS. Arterial blood volume in BAT, as a marker of tissue vascularity, was measured with $[^{15}O]H_2O$, along with glucose or fatty acid uptake using $[^{18}F]$2-fluoro-2-deoxy-D-glucose or 14(R,S)-$[^{18}F]$fluoro-6-thia-heptadecanoic acid PET imaging, respectively.

Results: BAT radiodensity was found to be correlating with tissue-retained blood and triglyceride content. Cold stimulus induced an increase in BAT radiodensity. Active BAT depots had higher radiodensity than both nonactive BAT and WAT. BAT radiodensity associated with systemic metabolic health parameters.

Conclusion: BAT radiodensity can be used as a marker of underlying tissue morphology. Active BAT can be identified using CT, exploiting tissue composition information. Moreover, BAT radiodensity provides an insight into whole-body systemic metabolic health. (*J Clin Endocrinol Metab* **102: 2258–2267, 2017**)

H uman adipose tissue is a complex organ with various physiological roles (1). White adipose tissue (WAT) predominantly serves as a reserve for stored lipids, whereas brown adipose tissue (BAT) is primarily known for a contributory role in nonshivering thermogenesis (2).

The composition and cellular characteristics of these adipose tissues are related with metabolic risk factors (3, 4). However, there are only limited methods to study adipose tissue composition noninvasively. X-ray computed tomography (CT) is a widely used *in vivo* imaging

technique in both clinical and experimental settings, although utility of CT beyond anatomical localization is still imprecise. CT radiodensity, measured in Hounsfield units (HUs), has been documented to be strongly related to biological tissue density (5, 6) and negative HU has been attributed with fat tissue (0 HU for water).

CT radiodensity measurements have been previously applied to liver (7), muscle (8), visceral (9) and epicardial (10) adipose tissue studies for the estimation of liver fat content, muscle triglyceride accumulation, and risks of development cardiovascular pathologies, respectively. Acute cold stimulus increases BAT HU (11–13), and cervico-thoracic fat depots with higher [^{18}F]2-fluoro-2-deoxy-D-glucose ([^{18}F]FDG) positron emission tomography (PET) standardized uptake value (SUV) have higher HU than depots with lower SUVs (14, 15). Moreover, Lee *et al.* (16) demonstrated $25 \pm 8\%$ increase in BAT radiodensity after 1-mo cold acclimation. In these BAT studies, radiodensity has been speculated to represent BAT triglyceride content. However, definite evidence is missing. Moreover, cutoff value for BAT in the HU scale proposed by Ahmadi *et al.* (14) to differentiate BAT from WAT needs further validation based on PET substrate tracer uptake values (17). Additionally, BAT triglyceride content, measured with ^{1}H-magnetic resonance spectroscopy (^{1}H-MRS), has been shown to associate with obesity markers and insulin sensitivity (18, 19), and it is critical to establish whether this holds true for triglyceride content measured with CT radiodensity, as CT is performed frequently in metabolic imaging studies for anatomical localization, and clinically it is a comparatively widely available tool compared with ^{1}H-MRS (20).

In this study, we hypothesize that CT radiodensity of human BAT at room temperature (RT) and cold associates with ^{1}H-MRS–measured BAT triglyceride content at RT, and PET-measured BAT retained blood volume at RT and cold; furthermore, BAT radiodensity increases as a result of cold stimulus. We additionally aimed to evaluate whether the differentiation of different fat depots can be done entirely based on their HU, and furthermore, whether BAT radiodensity is related to obesity markers and whole-body insulin sensitivity.

Materials and Methods

Study subjects

The subjects were recruited with newspaper and electronic adverts and were screened for hypertension (blood pressure >160/100 mm Hg), abnormal oral glucose tolerance test (2-hour oral glucose tolerance test >7.8 mmol/L), and cardiovascular status (arrhythmia and/or long Q wave and T wave in the heart's electric cycle in electrocardiogram, abnormal cardiac murmur, previous history of cardiovascular disease). Whole-body insulin sensitivity (M-value) was measured using hyperinsulinemic euglycemic clamp technique (21). After excluding smokers, pregnant females, patients

with diabetes, and subjects with ongoing medical conditions, 66 adult healthy human study subjects of both genders (45 females/21 males) participated in the study. The characteristics of study subjects have been given in Table 1. A written informed consent was obtained from all study subjects prior to inclusion in this study. This study was approved by the ethical review committee of Hospital District of Southwest Finland and carried out according to the principles of declaration of Helsinki, good medical practice and good clinical practice guidelines.

Study design

The study subjects underwent a series of scanning, as shown in our study protocol (Fig. 1). The subjects were scanned with PET-CT, in an individualized cold stimulus setting, in which part of the study subjects were scanned with a glucose analog [^{18}F]FDG radiotracer (n = 26) and another part of the study subjects were imaged using a fatty acid analog 14(R,S)-[^{18}F]fluoro-6-thia-heptadecanoic acid ([^{18}F]FTHA) radiotracer (n = 40). In the same scanning setting, [^{15}O]H$_2$O PET scans were also performed for the measurement of tissue-retained arterial blood volume (V$_A$). The CT and [^{15}O]H$_2$O PET scanning was repeated, on a separate day, at RT (22°C) in half of the study subjects (n = 33) as a comparative secondary parameter, whereas cold-stimulated BAT CT radiodensity is a primary evaluated parameter of the current study. The other half of the study participants (n = 33), who were not scanned with PET-CT at RT, were scanned with other interventions, answering different hypotheses (data to be reported elsewhere). Blood samples were drawn during the PET-CT scans to measure plasma concentration of glucose, nonesterified fatty acids (NEFAs), triglycerides, and thyroid hormones. Indirect calorimetry, using Deltatrac II Datex-Ohmeda, was performed during the PET-CT sessions to measure whole-body energy expenditure, according to Weir equation (22). During the cold stimulus PET-CT scanning sessions, the skin temperature of the subjects was monitored using a digital thermometer (Art.183; Termometerfabriken Viking AB, Eskilstuna, Sweden), in which the temperature-sensing probe was attached to the lateral abdominal skin surface. Additionally, in a separate scanning session, magnetic resonance proton spectroscopy (^{1}H-MRS) in the supraclavicular fat depot was performed at ambient RT for the determination of stored triglyceride. All the scanning sessions were performed after an overnight fasting. The scanning sessions were organized on separate days, in a random order, with the minimum interval between the sessions being 1 week.

Personalized cooling protocol

In the scans involving cold stimulus, the cold exposure was initiated 2 hours prior to the scan using cooling blankets (Blanketrol III; Cincinnati Sub-Zero, Cincinnati, OH) and cooling was continued, following the same protocol, during the scanning. The cooling was started with temperature of the water circulating the cooling blanket set to 4 to 6°C; this temperature was gradually raised once overt shivering was perceived by the subjects, either reported by the subject themselves or visually observed by the investigator. Supplemental Fig. 1 shows the temperature of the cooling blankets.

Scanning protocol

The CT scans were performed using low-dose scanner settings in which x-ray tube current was ~50 mA and tube voltage was 120 kVp. The [^{15}O]H$_2$O PET scans were conducted following intravenous injection of radiowater (500 MBq) and scanning

Table 1. Characteristics of Study Subjects

Parameter		Entire Cohort	Low-BAT	High-BAT	P Value	Cohen's d
			Groups Based on BAT Activity			
N		66	24	42	—	—
Gender		45 F/21 M	10 F/14 M	35 F/7 M	—	—
Age (y)		39.0 ± 9.8	43.4 ± 7.8	36.4 ± 10.1	0.005	0.78
BMI (kg/m^2)		25.4 ± 4.4	27.6 ± 5.4	24.2 ± 3.1	0.001	0.8
Waist (cm)		86.3 ± 15.8	93.1 ± 18.2	82.1 ± 12.5	0.006	0.72
Weight		74.2 ± 16.5	84.0 ± 19.1	68.6 ± 11.8	0.0001	0.99
Insulin sensitivity (M-value) (μmol/kg/min)		43.8 ± 20.8	36.8 ± 21.2	47.1 ± 19.4	0.065	0.51
Hip circumference (cm)		99.1 ± 10.7	102.8 ± 12.1	96.8 ± 9.1	0.03	0.57
Plasma triglycerides (mmol/L)		0.9 ± 0.6	1.0 ± 0.7	0.9 ± 0.6	0.13[a]	0.15
LDL cholesterol (mmol/L)		2.7 ± 0.7	2.9 ± 0.7	2.5 ± 0.7	0.035	0.57
HDL cholesterol (mmol/L)		1.7 ± 0.4	1.5 ± 0.3	1.8 ± 0.4	0.02	0.86
BAT NEFA uptake (μmol/100 g/min)		1.0 ± 0.1	0.4 ± 0.1	1.4 ± 1.0	<0.001	1.81
BAT glucose uptake (μmol/100 g/min)		7.4 ± 6.2	1.1 ± 0.6	9.7 ± 5.6	0.001	2.77
BAT [^{18}F]FDG SUV		2.1 ± 1.2	0.8 ± 0.2	2.5 ± 1.1	0.001	2.61
BAT stored triglyceride content (^{1}H-MRS) (percent)		79.2 ± 7.8	84.3 ± 3.4	75.6 ± 8.0	0.001	1.53
BAT blood perfusion (mL/100 g/min)	RT	7.4 ± 4.0	5.6 ± 3.6	8.8 ± 3.9	0.02	0.85
	Cold	13.1 ± 6.0[b]	10.4 ± 4.2[b]	14.6 ± 6.3[b]	0.007	0.80
BAT retained arterial blood (mL/100 g)	RT	2.3 ± 2.4	2.1 ± 1.6	2.5 ± 3.0	0.62	0.17
	Cold	6.3 ± 5.2[b]	3.5 ± 3.2	7.8 ± 5.5[b]	0.001	0.98
Whole-body energy expenditure (MJ/d)	RT	6.4 ± 1.3	7.1 ± 1.4	5.9 ± 1.1	0.01	0.96
	Cold	7.4 ± 1.6[b]	7.9 ± 1.6[b]	7.2 ± 1.5[b]	0.099	0.45
Change (Δ) in whole-body energy expenditure (MJ/d)		1.1 ± 0.2	1.3 ± 1.1	0.9 ± 1.1	0.41	0.36
Mean temperature of cooling blanket (°C)	0–60 min	5.6 ± 2.0	5.2 ± 1.5	6.0 ± 2.3	0.79	0.42
	60–120 min	8.8 ± 3.8	8.4 ± 4.2	9.1 ± 3.7	0.68	0.18
	120–180 min	11.8 ± 4.2	11.3 ± 5.2	12.2 ± 3.4	0.49	0.23

Data are shown as mean ± standard deviation. Low-BAT and high-BAT groups have been compared with independent sample Student t test, unless otherwise stated.

Abbreviations: BMI, body mass index; HDL, high-density lipoprotein; LDL, low-density lipoprotein; MJ, megajoules.

[a]Mann–Whitney U test.

[b]Significantly different from corresponding RT measurement in a paired analysis, P < 0.05, paired sample Student t test.

cervico-upper thoracic region with a dynamic acquisition protocol (6 × 5 seconds, 6 × 15 seconds, 6 × 30 seconds, 2 × 60 seconds). The [^{18}F]FDG and [^{18}F]FTHA PET scans were performed using a dynamic acquisition protocol (40 minutes; 4 × 30 seconds, 1 × 60 seconds, 1 × 120 seconds, 3 × 300 seconds, 2 × 600 seconds) following the administration of ~185 MBq radiotracer. ^{1}H-MRS measurements were performed at ambient RT in supraclavicular fat depot in 34 subjects (Fig. 1). The detailed description of ^{1}H-MRS measurements has been provided in Supplemental Material.

Image analysis

Carimas 2.8 software (Turku PET Centre, Turku, Finland) was used to analyze all acquired images. On CT images, all potential BAT locations within cervico-upper thoracic region were marked, and all voxels between −250 HU and −50 HU were thresholded (Supplemental Fig. 2). We also examined a bit wider range of HU threshold (−250 to 0 HU); however, visual inspection of those voxels revealed inclusion of nonadipose tissue structures, and therefore threshold upper-bound value of −50 HU was found to be reasonable. Muscle volumes of interests (VOIs) were drawn at the deltoid and pectoralis major region; and anterior subcutaneous fat in abdominal region was considered as WAT. Afterward, mean HU of all the regions of interest were calculated and compared. BAT glucose and fatty acid uptake was calculated by drawing VOIs on supraclavicular fat depots on [^{18}F]FDG PET and [^{18}F]FTHA

images, respectively. The generated time activity curves, from the drawn VOIs, were analyzed against radioactivity in arterial plasma using the Patlak linearization model (23). Tissue SUVs were calculated from [^{18}F]FDG PET scan at 30- to 40-minute time frame. Magnetic resonance spectroscopy data were quantified using LCModel (Supplemental Material). V_A in the fat depots was calculated from obtained time activity curves by drawing VOI at supraclavicular fat depot on [^{15}O]H$_2$O PET images and by assuming one tissue compartment model, as follows:

$$C_T(t) = K_1^W \cdot C_A(t) \otimes e^{-K2 \cdot t} + V_A \cdot C_A(t)$$

where C_T is the tissue time activity curve, C_A is the input function, V_A is the arterial blood volume, K_1^w is the influx of the tracer toward the tissue (perfusion), and k_2 is the out-flux of the tracer. The K_1^w, k_2, and V_A, values were estimated by a optimization procedure (Gauss-Newton method).

Statistical analyses

Statistical analyses were performed using IBM SPSS Statistics (version 22). Paired sampled Student t test was used to compare paired values, whereas independent sample t test was used to compare unrelated values. Effect sizes (Cohen's d) were calculated using an online statistical calculator (24). In correlation analysis, Pearson's correlation was used for normally distributed data sets, whereas Spearman's correlation test was used where the data failed the normality test. Multivariate linear
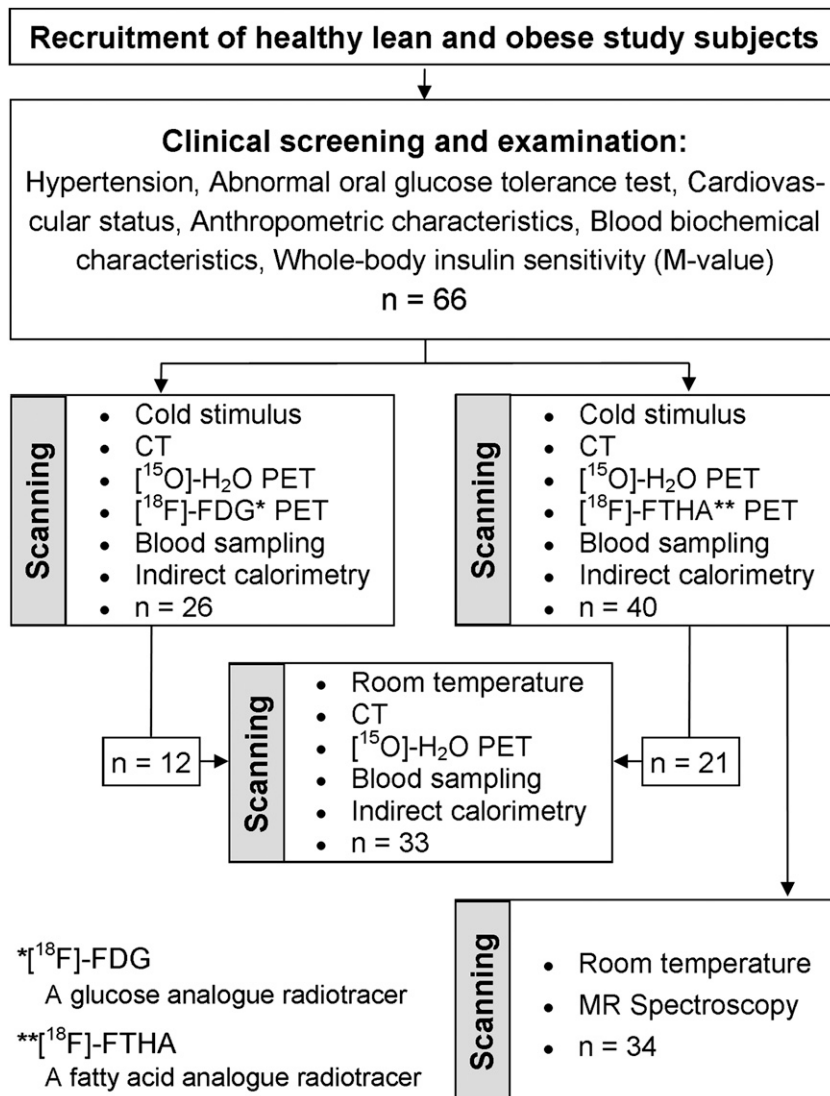
Figure 1. Display of the study design. Healthy lean and obese study subjects were recruited and screened for hypertension, abnormal oral glucose tolerance test, and cardiovascular status. Whole-body insulin sensitivity, blood biochemical characteristics, and anthropometric characteristics were also measured. The subjects underwent cold-stimulated PET-CT scans, in which part of the study subjects were scanned with a glucose analog [18F]FDG radiotracer (n = 26) and part of the study subjects were imaged using a fatty acid analog [18F]FTHA radiotracer (n = 40) using PET scanner. The [15O]H$_2$O PET radiotracer was also used, along with aforementioned tracers, for the measurement of tissue-retained V$_A$. The CT and [15O]H$_2$O PET scanning was repeated at RT in half of the study subjects (n = 33). Indirect calorimetry was performed during PET-CT scans. In a separate scanning session, ^{1}H-MRS of the supraclavicular fat depot at ambient RT was performed for the measurement of tissue-retained triglyceride content (n = 34).

regression analysis was used to evaluate whether the relationships between BAT radiodensity and whole-body insulin sensitivity, biochemical markers, and anthropometric measurements are independent of any covariates. Receiver-operating characteristic (ROC) plots were used to find an optimal cutoff limit on the HU scale for the differentiation of BAT from WAT (25). $P < 0.05$ was considered to be statistically significant.

Results

The whole-body energy expenditure was significantly higher during cold stimulus, compared with RT, which

signifies the effectiveness of used cooling protocol (RT: 6.4 ± 1.4 megajoules/d; cold: 7.4 ± 1.9 megajoules/d, $P < 0.001$). The subjects were classified, high-BAT or low-BAT, based on their BAT substrate tracer uptake (*i.e.*, metabolic activity; Table 1). They were categorized to be high-BAT if they had NEFA uptake of >0.7 μmol/100 g/min (median division) or glucose uptake of >3.0 μmol/100 g/min (26) within supraclavicular BAT depots. These selected substrate uptake threshold values are comparable in terms of energy content following complete oxidation.

Effect of cold stimulus on BAT radiodensity

A highly significant change in BAT radiodensity during RT (−85.09 ± 9.1 HU) and cold (−82.25 ± 9.1 HU) was observed [$P < 0.0001$, Cohen's $d = 0.90$; Fig. 2(a)], which was still persistent when subjects were categorized into high-BAT ($P = 0.001$, Cohen's $d = 0.93$) and low-BAT groups [$P = 0.001$, Cohen's $d = 1.11$; Fig. 2(b)]. Interestingly, high-BAT category had significantly higher radiodensity of BAT regions compared with low-BAT category both during RT and cold [$P < 0.001$, Cohen's $d = 1.05$, independent sample t test; Fig. 2(b)]. BAT radiodensity measured at RT and cold correlated significantly ($r = 0.94$, $P < 0.0001$). No significant difference in radiodensity was observed in WAT ($P = 0.47$), deltoid muscle ($P = 0.40$), and pectoralis major muscle [$P = 0.13$; Fig. 2(c)].

BAT radiodensity, V$_A$, stored triglyceride content, and local substrate uptake

Cold-activated BAT radiodensity correlated directly with tissue-retained V$_A$ measured with [15O]H$_2$O PET imaging [$rho = 0.32$, $P = 0.01$; Fig. 3(a)] and inversely with BAT-stored triglyceride content measured at RT with ^{1}H-MRS [$r = −0.51$, $P = 0.002$; Fig. 3(b)]. BAT radiodensity at RT also correlated with stored triglyceride content measured with ^{1}H-MRS ($r = −0.54$, $P = 0.02$). High-BAT subjects had significantly lower
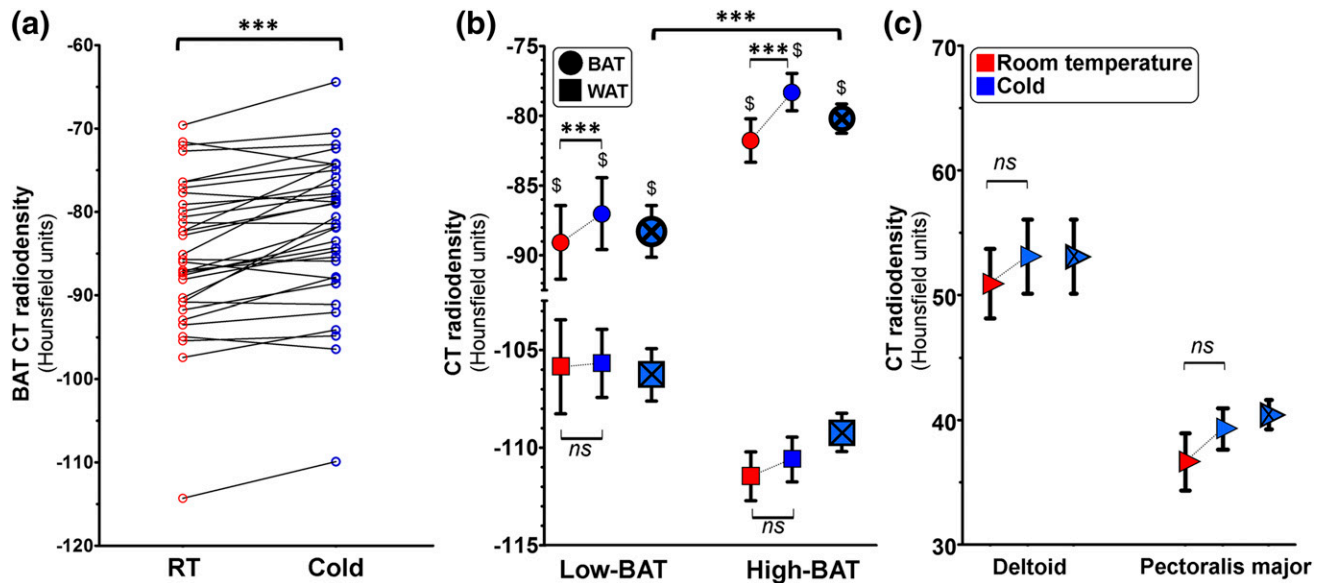
Figure 2. Effect of cold stimulus on radiodensity. (a) BAT radiodensity, expressed as HU, during RT and after cold stimulation, increased significantly (paired Student t test, ***P < 0.001, n = 33). (b) Change in BAT (●) and WAT (■) radiodensity both in low-BAT (paired Student t test, BAT: ***P = 0.001; WAT: P = 0.70, n = 15) and high-BAT (paired Student t test, BAT: ***P = 0.001; WAT: P = 0.55, n = 18) categories. Significant difference in cold-activated BAT radiodensity was found in both groups (independent sample t test, ***P < 0.001, Cohen's d = 1.05, low-BAT: n = 24, high-BAT: n = 42). $^{\$}$Shows the significant difference (all P < 0.01, paired Student t test) between corresponding BAT and WAT radiodensity measurements. (c) Change in radiodensity within deltoid muscle (paired Student t test, P = 0.40, n = 33) and pectoralis major muscle (paired Student t test, P = 0.13, n = 33) during RT and cold. Data are shown as mean ± standard error of the mean. The dotted lines show the paired readings. The readings with a cross sign x represent the mean ± standard error of the mean of the entire cohort. ns, nonsignificant.

triglyceride content than low-BAT subjects measured with ^{1}H-MRS (P = 0.001; Table 1). Furthermore, V_A in BAT depots was significantly higher during cold stimulus (6.3 ± 5.2 mL/100 g) compared with RT (2.3 ± 2.4 mL/100 g, P < 0.001, Cohen's d = 0.86). Moreover, the change (Δ) in V_A and the change (Δ) in BAT radiodensity correlated significantly (r = 0.44, P = 0.01; Supplemental Fig. 3), indicating the phenomena of increased
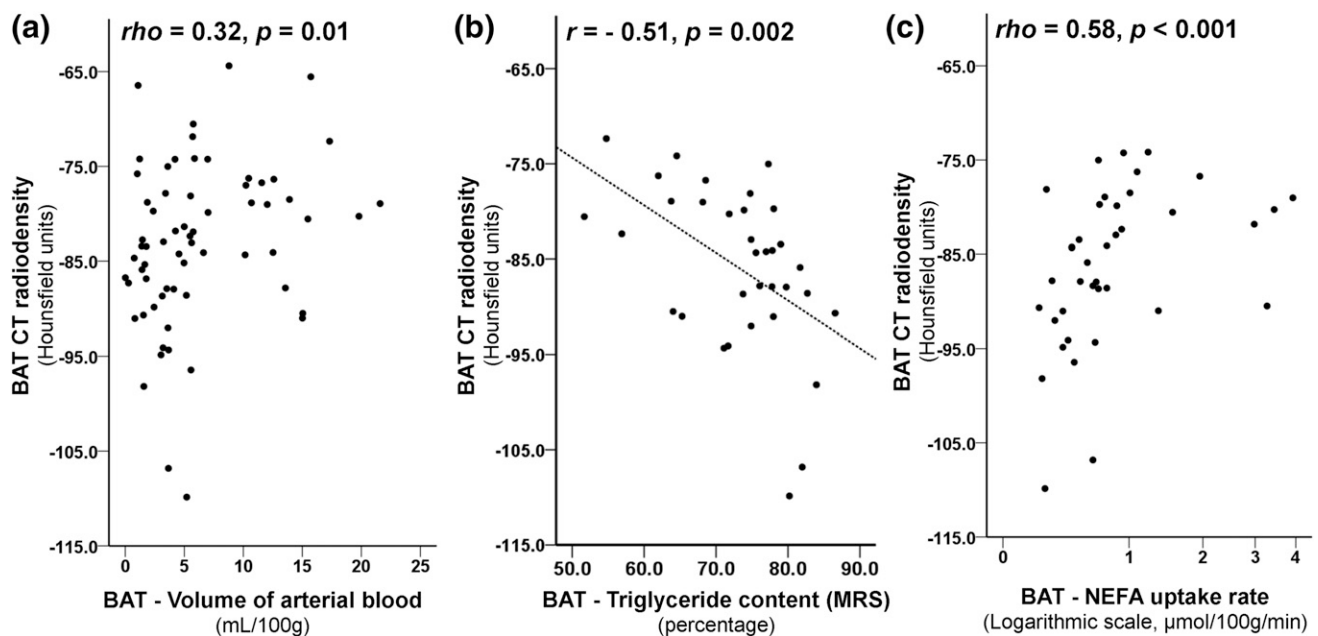

Figure 3. Radiodensity as a marker of tissue composition. (a) Significant positive correlation between BAT radiodensity and tissue-retained volume of arterial blood measured with [^{15}O]H$_2$O PET imaging during cold (Spearman's rho = 0.32, P = 0.01, n = 65). (b) Significant negative correlation between cold-activated BAT radiodensity and triglyceride content measured with ^{1}H-MRS in RT (Pearson's r = − 0.51, P = 0.002, n = 34). (c) Significant positive relationship between cold-stimulated BAT CT radiodensity and BAT NEFA uptake rate (Spearman's rho = 0.58; P < 0.001, n = 39); BAT NEFA uptake data have been shown in logarithmic scale due to nonnormal distribution.

tissue-retained blood content during cold due to higher blood perfusion is likely to be a factor for the change in BAT radiodensity after a cold stimulus. Interestingly, we also found a significant positive correlation between cold-activated BAT radiodensity and NEFA uptake rate [$rho = 0.58$, $P < 0.001$, n = 39; Fig. 3(c)]. There was no linear relationship between BAT glucose uptake and CT HU [$rho = 0.16$, $P = 0.44$; Supplemental Fig. 4(a)]. We further investigated the relationship of cold-activated BAT SUV_{mean}, a conventional marker for glucose consumption, with BAT radiodensity; however, no such relationship was found [$r = 0.12$, $P = 0.55$; Supplemental Fig. 4(b)]. There was a highly linear direct relationship between cold-activated BAT glucose uptake and BAT SUV_{mean} [$r = 0.96$, $P < 0.0001$; Supplemental Fig. 4(c)].

BAT radiodensity and systemic metabolic health markers

Cold-activated BAT radiodensity was in negative relationship with obesity markers, *i.e.*, body mass index (BMI; $r = -0.71$, $P < 0.001$), waist circumference [$r = -0.75$, $P < 0.0001$; Fig. 4(a)], and hip circumference ($r = -0.62$, $P < 0.0001$). These relationships remained significant when adjusted for age in multivariate linear regression analysis. Furthermore, cold-activated BAT radiodensity also correlated with cold-stimulated plasma triglyceride levels ($r = -0.54$, $P = 0.001$, n = 37) as well as RT plasma triglycerides [$rho = -0.46$, $P < 0.001$, n = 64; Fig. 4(b)], low-density lipoprotein (LDL; $rho = -0.34$,

$P = 0.007$), and high-density lipoprotein (HDL; $rho = 0.37$, $P = 0.003$). However, these BAT CT radiodensity relationships with plasma triglycerides, LDL, and HDL lost statistical significance once adjusted for BMI. Moreover, there was also positive correlation between whole-body insulin sensitivity (M-value) and BAT CT radiodensity during cold [$r = 0.49$, $P < 0.001$; Fig. 4(c)] and RT ($r = 0.48$, $P = 0.007$); this association remained significant when adjusted separately for BMI ($\beta = 1.3 \pm 0.4$ µmol/kg/min/HU, $P = 0.002$), waist circumference ($\beta = 1.0 \pm 0.4$ µmol/kg/min/HU, $P = 0.02$), sex ($\beta = 1.1 \pm 0.3$ µmol/kg/min/HU, $P = 0.0002$), or age ($\beta = 1.2 \pm 0.3$ µmol/kg/min/HU, $P < 0.001$) in multivariate linear regression analysis. Whole-body insulin sensitivity (M-value) also directly correlated with muscle radiodensity (deltoid: $rho = 0.32$, $P = 0.01$; pectoralis major: $r = 0.29$, $P = 0.02$), whereas no relation was found with WAT radiodensity ($r = 0.18$, $P = 0.18$). Table 2 shows correlation coefficients of BAT CT radiodensity, both RT and cold, with biochemical markers and anthropometric measurements.

Subcutaneous WAT and BAT radiodensity

Low-BAT and high-BAT groups had higher HU in the BAT depots compared with corresponding WAT at RT (low-BAT: $P = 0.001$, Cohen's $d = 2.09$; high-BAT: $P < 0.0001$, Cohen's $d = 3.78$) as well as during cold [low-BAT: $P < 0.001$, Cohen's $d = 2.02$; high-BAT: $P < 0.0001$, Cohen's $d = 4.08$; Fig. 2(b)]. ROC curves were plotted to predict the ability of HU, and to find an optimal
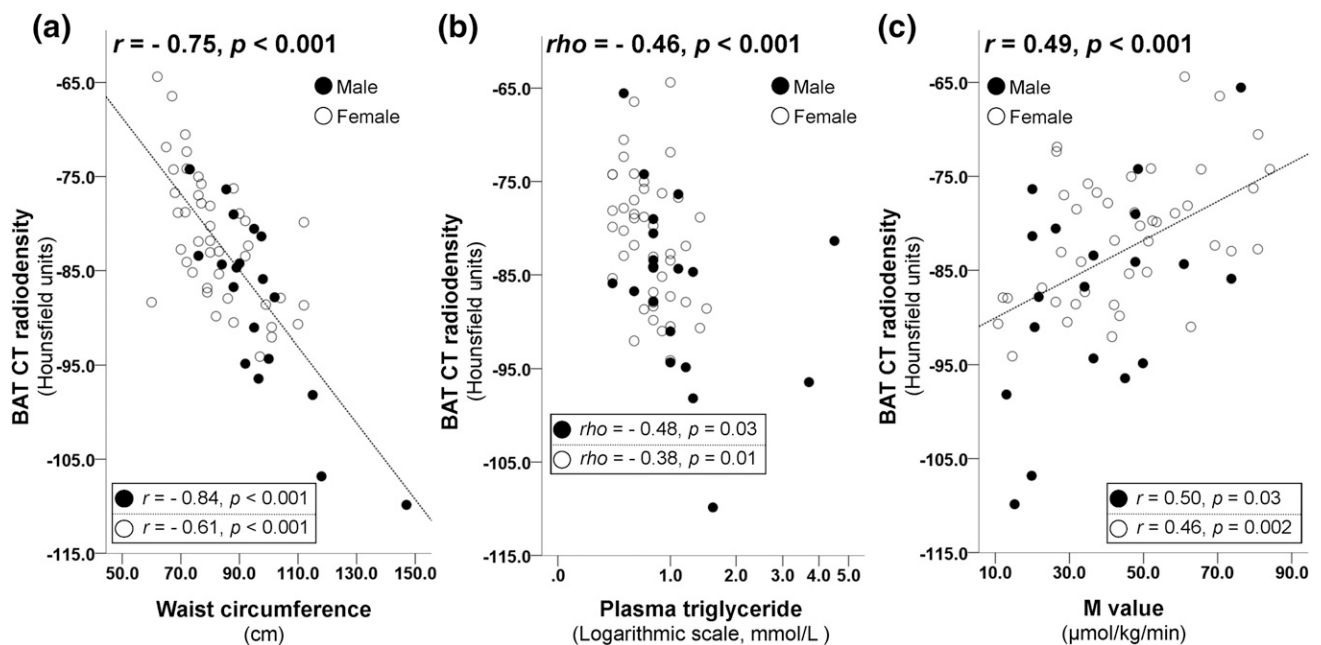

Figure 4. Cold-stimulated BAT radiodensity and metabolic health parameters. (a) Negative correlation between cold-stimulated BAT CT radiodensity and waist circumference. (b) Inverse relationship between cold-stimulated BAT CT radiodensity and RT plasma triglycerides (n = 64). RT plasma triglyceride levels ranged from 0.4 to 4.5 mmol/L (median: 0.8). The data have been shown in logarithmic scale due to nonnormal distribution. (c) Direct relationship between BAT CT radiodensity during cold and whole-body insulin sensitivity (M-value, n = 63).

Table 2.   Correlation of BAT CT Radiodensity With Anthropometric Measurements and Biochemical Markers

| | BAT CT Radiodensity (HU) | | | |
| | RT | | Cold Stimulus | |
Variable	Correlation Coefficient	P Value	Correlation Coefficient	P Value
Age	−0.16	0.36	−0.28	0.02
Sex (M = 1, F = 2)	0.42	0.02	0.32	0.009
BMI	−0.82	<0.001	−0.71	<0.001
Weight	−0.83	<0.001	−0.70	<0.001
Waist circumference	−0.88	<0.001	−0.75	<0.001
Hip circumference	−0.72	<0.001	−0.62	<0.001
M-value	0.48	0.007	0.49	<0.001
Plasma triglyceride (RT)	−0.48[a]	0.005	−0.46[a]	<0.001
Plasma triglyceride (cold)	−0.61	0.003	−0.54	0.001
LDL	−0.35	0.048	−0.34[a]	0.007
HDL	0.61[a]	<0.001	0.37[a]	0.003
Total cholesterol	−0.03	0.89	−0.23	0.07

[a]Spearman's correlation coefficient.

cutoff point on HU scale, first to differentiate BAT from WAT [Supplemental Fig. 5(a)] and second high-BAT depots from both low-BAT and WAT depots [Supplemental Fig. 5(b)]. Area under the ROC curve (±standard error) to differentiate BAT from WAT was 0.98 ± 0.01 [$P < 0.001$; Supplemental Fig. 5(a)], and area under the ROC curve (±standard error) to predict high-BAT was 0.93 ± 0.02 [$P < 0.001$; Supplemental Fig. 5(b)]. Based on this, we found the optimal cutoff point on HU scale to be highly specific (100%) for WAT at ≤−92.4 HU (sensitivity 89%), and the optimal cutoff point on HU scale of fat depot to be high-BAT, under cold stimulus, at ≥−87 HU (sensitivity 83%, specificity 87%).

Discussion

Our data show that BAT CT radiodensity is a potential marker of BAT triglyceride content and tissue-retained V_A. Furthermore, cold stimulus results in an increase in BAT radiodensity, which is most likely due to an increase in tissue-retained blood volume as a result of cold-induced tissue hyperperfusion. BAT regions with higher radiodensity, under cold stimulation, take up more NEFA from circulation than those with lower radiodensity, and BAT regions with mean radiodensity of ≥−87 HU are likely to be metabolically active. BAT radiodensity is significantly higher than subcutaneous WAT, and radiodensity of ≤−92.4 HU is highly specific for WAT. Moreover, BAT radiodensity has significant relationship with obesity markers (BMI, waist circumference, hip circumference, plasma triglyceride, HDL, LDL) and whole-body insulin sensitivity.

Previously, it has been shown that BAT perfusion increases during cold stimulus (26, 27), and BAT substrate metabolism increases in uncoupling protein

1–mediated thermogenesis (12, 28). Under cold stimulus, BAT increases its retained volume of arterial blood (Table 1), and BAT-stored triglyceride content decreases due to lipolysis, most likely to fuel BAT-associated nonshivering thermogenesis (29, 30). It is a limitation of our study design that ^{1}H-MRS acquisition was performed solely at RT, and we cannot demonstrate cold-induced reduction in stored triglycerides with ^{1}H-MRS; however, some studies suggest this phenomenon (11, 31, 32). We showed in our study that the increase in BAT radiodensity [Fig. 2(a)] is due to the increase in tissue blood retention in cold, and we speculate that it may also be due to reduction in BAT triglycerides. Interestingly, this increase in radiodensity was also evident in subjects with low BAT substrate uptake (low-BAT). It is possible that low-BAT subjects have merely reduced substrate uptake, and in these fat depots there are still adipocytes with uncoupling protein 1, as shown by Lee *et al.* (33). HU does not explicitly measure stored triglyceride content in fat depots but also water, blood, and residual fat cell components. It has been shown that obese individuals are attributed to lower fat tissue–retained water content, lower fat depot capillary bed density (34), and overall adipocyte hypertrophy (35). Moreover, fat depots with high metabolic activity are also densely packed with mitochondria (36). Low-BAT subjects in our cohort are comparatively obese (Table 1); therefore, the lower BAT radiodensity in low-BAT subjects compared with high-BAT subjects may be accounted for in these morphological differences. Additionally, the differences in BAT radiodensity in our low-BAT and high-BAT group are in line with the previous finding by Hu *et al.* (15), in which it has been shown that metabolically active supraclavicular, interscapular, and neck fat, based on [^{18}F]FDG SUVs, has higher CT radiodensity than inactive fat.

We found a significant association between BAT CT radiodensity and BAT NEFA uptake rate [Fig. 3(c)], which implies that either BAT regions with lower triglyceride content take up more NEFA from circulation in cold to fulfill their energy needs or these regions have higher ratio of brown adipocytes to white adipocytes. However, it is not clear whether these NEFAs are used for thermogenesis or replenishment of used triglycerides, which should be assessed with further biochemical and histological studies.

BAT radiodensity correlates inversely with obesity, LDL cholesterol, and plasma triglycerides, and positively with whole-body insulin sensitivity (M-value) and HDL cholesterol. These results are in line with previous findings by Raiko et al. (19), who measured BAT triglyceride content using magnetic resonance spectroscopy. It has been shown in numerous earlier studies that intramuscular triglyceride stores have relationship with insulin sensitivity (37, 38), and, in line with this, we found relationships of whole-body insulin sensitivity with radiodensity of deltoid and pectoralis major muscle. However, BAT triglyceride content associated with whole-body insulin sensitivity in a study by Raiko et al. (19) using magnetic resonance spectroscopy, whereas we show similar results with BAT CT attenuation, further supporting the link between whole-body insulin sensitivity and BAT composition. Cervico-thoracic BAT depots with thermogenic, lipogenic, and lipolytic activity have a potential role in regulating plasma fatty acids, whereas high lipolysis with high plasma levels of free fatty acids can induce muscle insulin resistance (39). It has also been demonstrated in rodent studies that BAT contributes to plasma triglyceride clearance (40). Additionally, human studies of both healthy (16) and type II diabetic subjects (41) have shown that a short-term cold acclimation increases BAT radiodensity, and cold acclimation improves insulin sensitivity in patients with type 2 diabetes (41). However, our study does not include subjects with diabetes, but, in line with these findings, our results demonstrate another evidence for the link of BAT CT radiodensity with insulin sensitivity independent of age, sex, or obesity. Future studies with longitudinal design may unravel the casual link between BAT and whole-body insulin sensitivity.

A few previous studies (14, 31) compared BAT and WAT radiodensity in subjects with high SUV supraclavicular fat depots (high-BAT) with similar results as in the current report. However, to our knowledge, no other study has statistically compared HU of WAT and BAT in low-BAT study subjects. Our data suggest that BAT area in low-BAT subjects still differs from subcutaneous WAT on HU scale. This difference could be due to higher fluid-to-triglyceride ratio in BAT regions in low-BAT subjects compared with corresponding subcutaneous WAT.

Strengths of our study include that all study subjects were metabolically healthy and had broad-ranging BMI and age, and the cohort included both genders. However, our cohort had more females than males, which limits our gender-based analyses. These findings are expected to aid future BAT studies and provide more insight in *in vivo* assessment of intracellular triglyceride accumulation in supraclavicular fat depot as a marker of BAT activity, obesity, and whole-body insulin sensitivity. In clinical setting, with CT being a routinely performed procedure, BAT radiodensity may allow additional information about systemic metabolic health.

The aim of our personalized cooling protocol was to deliver uniform level of nonshivering cold stress in all participants irrespective of body type and subcutaneous adiposity; however, our method for the assessment of shivering was subjective. An objective and quantitative approach to detect shivering, *e.g.*, electromyography, would have improved this protocol. Although we did not observe the difference in change (Δ) in whole-body energy expenditure in high-BAT and low-BAT participants, there is a possibility that present cooling protocol may deliver cold stress of variable magnitude in different subjects, which may create a bias in cooling response of each subject. Furthermore, our study cannot establish causal relationship between BAT radiodensity and development of metabolic syndrome due to the cross-sectional study setting. Moreover, classification of subjects being high-BAT was solely done on PET substrate tracer uptake values during cold stimulation, and not on any *ex vivo* BAT-specific morphological or biochemical analysis. However, similar classification approach has previously been adapted and reported in several BAT reports (11, 18, 26, 42–44), and high PET substrate tracer values in fat depots to be specific for BAT have been previously demonstrated (36), and it is considered the golden standard for *in vivo* BAT localization.

Conclusions

We conclude that CT radiodensity of human BAT can be used as a marker of stored triglyceride content and local vascularity. Acute cold exposure significantly increases BAT CT radiodensity, which is most likely due to tissue hyperemia, and may also be as a result of reduction in intracellular lipids. Cold-stimulated BAT with high substrate uptake has higher radiodensity than those with lower uptake levels. Cervico-upper thoracic fat depots with more positive HU (in fat HU range) than typical subcutaneous WAT under cold stimulus are most likely metabolically active based on PET imaging. Furthermore, BAT triglyceride accumulation assessed with HU may provide an insight in whole-body insulin sensitivity and

systemic metabolic health, which may further broaden the utilization of CT beyond anatomical imaging.

Acknowledgments

References

1. Bjorndal B, Burri L, Staalesen V, Skorve J, Berge RK. Different adipose depots: their role in the development of metabolic syndrome and mitochondrial response to hypolipidemic agents. *J Obes*. 2011;**2011**:490650.
2. Cinti S. The role of brown adipose tissue in human obesity. *Nutr Metab Cardiovasc Dis*. 2006;**16**(8):569–574.
3. Salans LB, Knittle JL, Hirsch J. The role of adipose cell size and adipose tissue insulin sensitivity in the carbohydrate intolerance of human obesity. *J Clin Invest*. 1968;**47**(1):153–165.
4. Weyer C, Foley JE, Bogardus C, Tataranni PA, Pratley RE. Enlarged subcutaneous abdominal adipocyte size, but not obesity itself, predicts type II diabetes independent of insulin resistance. *Diabetologia*. 2000;**43**(12):1498–1506.
5. Ciarelli MJ, Goldstein SA, Kuhn JL, Cody DD, Brown MB. Evaluation of orthogonal mechanical properties and density of human trabecular bone from the major metaphyseal regions with materials testing and computed tomography. *J Orthop Res*. 1991;**9**(5):674–682.
6. McBroom RJ, Hayes WC, Edwards WT, Goldberg RP, White AA III. Prediction of vertebral body compressive fracture using quantitative computed tomography. *J Bone Joint Surg Am*. 1985;**67**(8):1206–1214.
7. Shores NJ, Link K, Fernandez A, Geisinger KR, Davis M, Nguyen T, Sawyer J, Rudel L. Non-contrasted computed tomography for the accurate measurement of liver steatosis in obese patients. *Dig Dis Sci*. 2011;**56**(7):2145–2151.
8. Anderson DE, D'Agostino JM, Bruno AG, Demissie S, Kiel DP, Bouxsein ML. Variations of CT-based trunk muscle attenuation by age, sex, and specific muscle. *J Gerontol A Biol Sci Med Sci*. 2013;**68**(3):317–323.
9. Rosenquist KJ, Pedley A, Massaro JM, Therkelsen KE, Murabito JM, Hoffmann U, Fox CS. Visceral and subcutaneous fat quality and cardiometabolic risk. *JACC Cardiovasc Imaging*. 2013;**6**(7):762–771.
10. Pracon R, Kruk M, Kepka C, Pregowski J, Opolski MP, Dzielinska Z, Michalowska I, Chmielak Z, Demkow M, Ruzyłło W. Epicardial adipose tissue radiodensity is independently related to coronary atherosclerosis: a multidetector computed tomography study. *Circ J*. 2011;**75**(2):391–397.
11. Baba S, Jacene HA, Engles JM, Honda H, Wahl RL. CT Hounsfield units of brown adipose tissue increase with activation: preclinical and clinical studies. *J Nucl Med*. 2010;**51**(2):246–250.
12. Ouellet V, Labbé SM, Blondin DP, Phoenix S, Guérin B, Haman F, Turcotte EE, Richard D, Carpentier AC. Brown adipose tissue oxidative metabolism contributes to energy expenditure during acute cold exposure in humans. *J Clin Invest*. 2012;**122**(2):545–552.
13. Blondin DP, Labbé SM, Phoenix S, Guérin B, Turcotte ÉE, Richard D, Carpentier AC, Haman F. Contributions of white and brown adipose tissues and skeletal muscles to acute cold-induced metabolic responses in healthy men. *J Physiol*. 2015;**593**(3):701–714.
14. Ahmadi N, Hajsadeghi F, Conneely M, Mingos M, Arora R, Budoff M, Ebrahimi R. Accurate detection of metabolically active "brown" and "white" adipose tissues with computed tomography. *Acad Radiol*. 2013;**20**(11):1443–1447.
15. Hu HH, Chung SA, Nayak KS, Jackson HA, Gilsanz V. Differential computed tomographic attenuation of metabolically active and inactive adipose tissues: preliminary findings. *J Comput Assist Tomogr*. 2011;**35**(1):65–71.
16. Lee P, Smith S, Linderman J, Courville AB, Brychta RJ, Dieckmann W, Werner CD, Chen KY, Celi FS. Temperature-acclimated brown adipose tissue modulates insulin sensitivity in humans. *Diabetes*. 2014;**63**(11):3686–3698.
17. van der Lans AA, Wierts R, Vosselman MJ, Schrauwen P, Brans B, van Marken Lichtenbelt WD. Cold-activated brown adipose tissue in human adults: methodological issues. *Am J Physiol Regul Integr Comp Physiol*. 2014;**307**(2):R103–R113.
18. Matsushita M, Yoneshiro T, Aita S, Kameya T, Sugie H, Saito M. Impact of brown adipose tissue on body fatness and glucose metabolism in healthy humans. *Int J Obes*. 2014;**38**(6):812–817.
19. Raiko J, Holstila M, Virtanen KA, Orava J, Saunavaara V, Niemi T, Laine J, Taittonen M, Borra RJ, Nuutila P, Parkkola R. Brown adipose tissue triglyceride content is associated with decreased insulin sensitivity, independently of age and obesity. *Diabetes Obes Metab*. 2015;**17**(5):516–519.
20. Eurostat. Healthcare resource statistics: technical resources and medical technology. Available at: http://ec.europa.eu/eurostat/statistics-explained/index.php/Healthcare_resource_statistics_-_technical_resources_and_medical_technology. Accessed 10 January 2015.
21. DeFronzo RA, Tobin JD, Andres R. Glucose clamp technique: a method for quantifying insulin secretion and resistance. *Am J Physiol*. 1979;**237**(3):E214–E223.
22. Weir JB. New methods for calculating metabolic rate with special reference to protein metabolism. *J Physiol*. 1949;**109**(1-2):1–9.
23. Patlak CS, Blasberg RG. Graphical evaluation of blood-to-brain transfer constants from multiple-time uptake data: generalizations. *J Cereb Blood Flow Metab*. 1985;**5**(4):584–590.
24. Wiseheart M. Effect size calculator. Available at: http://www.cognitiveflexibility.org/effectsize/. Accessed 12 March 2014.
25. Zweig MH, Campbell G. Receiver-operating characteristic (ROC) plots: a fundamental evaluation tool in clinical medicine. *Clin Chem*. 1993;**39**(4):561–577.
26. Orava J, Nuutila P, Lidell ME, Oikonen V, Noponen T, Viljanen T, Scheinin M, Taittonen M, Niemi T, Enerbäck S, Virtanen KA. Different metabolic responses of human brown adipose tissue to activation by cold and insulin. *Cell Metab*. 2011;**14**(2):272–279.
27. U Din M, Raiko J, Saari T, Kudomi N, Tolvanen T, Oikonen V, Teuho J, Sipilä HT, Savisto N, Parkkola R, Nuutila P, Virtanen KA. Human brown adipose tissue [(15)O]O2 PET imaging in the presence and absence of cold stimulus. *Eur J Nucl Med Mol Imaging*. 2016;**43**(10):1878–1886.
28. Richard D, Picard F. Brown fat biology and thermogenesis. *Front Biosci (Landmark Ed)*. 2011;**16**:1233–1260.

29. Geerling JJ, Boon MR, Kooijman S, Parlevliet ET, Havekes LM, Romijn JA, Meurs IM, Rensen PC. Sympathetic nervous system control of triglyceride metabolism: novel concepts derived from recent studies. *J Lipid Res*. 2014;**55**(2):180–189.

30. Blondin DP, Frisch F, Phoenix S, Guérin B, Turcotte ÉE, Haman F, Richard D, Carpentier AC. Inhibition of intracellular triglyceride lipolysis suppresses cold-induced brown adipose tissue metabolism and increases shivering in humans. *Cell Metab*. 2017;**25**(2):438–447.

31. Gifford A, Towse TF, Walker RC, Avison MJ, Welch EB. Characterizing active and inactive brown adipose tissue in adult humans using PET-CT and MR imaging. *Am J Physiol Endocrinol Metab*. 2016;**311**(1):E95–E104.

32. Lundström E, Strand R, Johansson L, Bergsten P, Ahlström H, Kullberg J. Magnetic resonance imaging cooling-reheating protocol indicates decreased fat fraction via lipid consumption in suspected brown adipose tissue. *PLoS One*. 2015;**10**(4):e0126705.

33. Lee P, Zhao JT, Swarbrick MM, Gracie G, Bova R, Greenfield JR, Freund J, Ho KK. High prevalence of brown adipose tissue in adult humans. *J Clin Endocrinol Metab*. 2011;**96**(8):2450–2455.

34. Pasarica M, Sereda OR, Redman LM, Albarado DC, Hymel DT, Roan LE, Rood JC, Burk DH, Smith SR. Reduced adipose tissue oxygenation in human obesity: evidence for rarefaction, macrophage chemotaxis, and inflammation without an angiogenic response. *Diabetes*. 2009;**58**(3):718–725.

35. Anand SS, Tarnopolsky MA, Rashid S, Schulze KM, Desai D, Mente A, Rao S, Yusuf S, Gerstein HC, Sharma AM. Adipocyte hypertrophy, fatty liver and metabolic risk factors in South Asians: the Molecular Study of Health and Risk in Ethnic Groups (molSHARE). *PLoS One*. 2011;**6**(7):e22112.

36. Virtanen KA, Lidell ME, Orava J, Heglind M, Westergren R, Niemi T, Taittonen M, Laine J, Savisto NJ, Enerbäck S, Nuutila P. Functional brown adipose tissue in healthy adults. *N Engl J Med*. 2009;**360**(15):1518–1525.

37. Forouhi NG, Jenkinson G, Thomas EL, Mullick S, Mierisova S, Bhonsle U, McKeigue PM, Bell JD. Relation of triglyceride stores in skeletal muscle cells to central obesity and insulin sensitivity in European and South Asian men. *Diabetologia*. 1999;**42**(8):932–935.

38. Larson-Meyer DE, Smith SR, Heilbronn LK, Kelley DE, Ravussin E, Newcomer BR; Look AHEAD Adipose Research Group. Muscle-associated triglyceride measured by computed tomography and magnetic resonance spectroscopy. *Obesity (Silver Spring)*. 2006;**14**(1):73–87.

39. Kelley DE, Mokan M, Simoneau JA, Mandarino LJ. Interaction between glucose and free fatty acid metabolism in human skeletal muscle. *J Clin Invest*. 1993;**92**(1):91–98.

40. Bartelt A, Bruns OT, Reimer R, Hohenberg H, Ittrich H, Peldschus K, Kaul MG, Tromsdorf UI, Weller H, Waurisch C, Eychmüller A, Gordts PL, Rinninger F, Bruegelmann K, Freund B, Nielsen P, Merkel M, Heeren J. Brown adipose tissue activity controls triglyceride clearance. *Nat Med*. 2011;**17**(2):200–205.

41. Hanssen MJ, Hoeks J, Brans B, van der Lans AA, Schaart G, van den Driessche JJ, Jörgensen JA, Boekschoten MV, Hesselink MK, Havekes B, Kersten S, Mottaghy FM, van Marken Lichtenbelt WD, Schrauwen P. Short-term cold acclimation improves insulin sensitivity in patients with type 2 diabetes mellitus. *Nat Med*. 2015;**21**(8):863–865.

42. Muzik O, Mangner TJ, Granneman JG. Assessment of oxidative metabolism in brown fat using PET imaging. *Front Endocrinol (Lausanne)*. 2012;**3**:15.

43. Muzik O, Mangner TJ, Leonard WR, Kumar A, Janisse J, Granneman JG. 15O PET measurement of blood flow and oxygen consumption in cold-activated human brown fat. *J Nucl Med*. 2013;**54**(4):523–531.

44. Yoneshiro T, Aita S, Matsushita M, Kameya T, Nakada K, Kawai Y, Saito M. Brown adipose tissue, whole-body energy expenditure, and thermogenesis in healthy adult men. *Obesity (Silver Spring)*. 2011;**19**(1):13–16.